Inorganic Chemistry

ARTICLE

pubs.acs.org/IC

Redox Properties of Tanaka's Water Oxidation Catalyst: Redox Noninnocent Ligands Dominate the Electronic Structure and Reactivity

Soumya Ghosh and Mu-Hyun Baik*

Department of Chemistry, Indiana University, 800 East Kirkwood Avenue, Bloomington, Indiana 47405, United States

Supporting Information

ABSTRACT: $[Ru_2(OH)_2(3,6\text{-}^tBu_2Q)_2(btpyan)]^{2+}$ ($^tBu_2Q$, 3,6-di-*tert*-butyl-1,2-benzoquinone; btpyan, 1,8-bis(2,2′:6′,2″-terpyridyl)-anthracene) is one of a handful of structurally well-defined homogeneous catalysts that can electrocatalytically oxidize water at room temperature. Unfortunately, the exact composition and the chemical properties of the redox intermediates leading to the catalytically competent species remains poorly resolved. On the basis of the UV−vis spectra the catalyst was previously speculated to lose two protons spontaneously to form an intermediate containing the key O−O bond in water. We evaluated this mechanistic scenario computationally and found that the associated pK_a values are in the range of 21, much too high to justify spontaneous deprotonation under experimental conditions of pH = 4. In later work, the O−O bond formation was speculated to occur after removal of two protons and two electrons. Extensive exploration of the various oxidation and protonation states that the diruthenium complex may access during catalyst activation reveals surprisingly complex electronic structure patterns in several redox intermediates: the quinone and tpy ligands become redox noninnocent, i.e., they participate actively in the electron transfer processes by temporarily storing redox equivalents. On the basis of this new insight into the electronic structure we propose a novel alternative explanation of the spectroscopic observations reported previously and characterize the electronic structure of the key intermediates in detail. Finally, the redox potential for the first two-electron oxidation is evaluated based on our proposed intermediates and predicted to be 0.411 V, which compares well with the experimentally observed broad two-electron wave at ∼0.32 V.

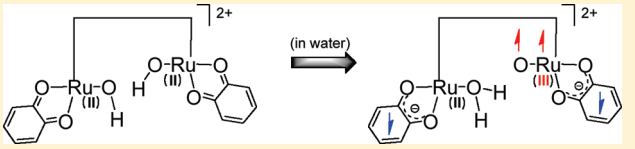

INTRODUCTION

The rapidly depleting reserves of easily accessible fossil fuel feed stocks add urgency to the long-standing challenge of developing new, sustainable technologies for alternative energy. The most viable solution to the energy crisis is the utilization of solar energy[1,2] with artificial photosynthesis being perhaps the most elegant of potential solutions. Nature utilizes a complex machinery including photosystems I and II to convert solar into chemical energy where the oxidation of water to dioxygen[3−5] serves as an inexhaustible source for electrons and protons that are ultimately used to reduce carbon dioxide. Among the technologies that must be developed to construct a device capable of artificial photosynthesis,[6,7] efficient and robust water oxidation catalysis under mild conditions has been particularly challenging to achieve. The *blue dimer*[8] was one of the first well-defined metal complexes capable of oxidizing water, and it has inspired many analogous systems.[9−20] Many of these complexes use Ru as the metal center with fairly innocent auxiliary ligands, and most of the key chemical steps are believed to take place at the metal.[21] The high oxidation state that may be accessed as a result of the removal of four electrons is problematic as it may lead to structural damage of the catalyst. In our previous work, we found that the electronic stress in the $Ru^V{=}O$ moiety of the catalytically active intermediate of the *blue dimer* gives rise to an intramolecular electron transfer to afford a $Ru^{IV}{-}O^{\bullet}$ fragment that is responsible for activating the O−H bond of water. Whereas the metal-induced spin polarization on the oxo ligand was constructive in this case, it is easy to envision destructive effects emerging from metal-induced modifications of ligand electronics.[22] Thus, it is important to understand how redox catalysts can mediate and dissipate charge-induced electronic stress. The catalyst reported by Tanaka et al.[23,24] $[Ru_2(OH)_2(3,6\text{-}^tBu_2Q)_2(btpyan)]^{2+}$ ($^tBu_2Q$, 3,6-di-*tert*-butyl-1,2-benzoquinone; btpyan, 1,8-bis(2,2′:6′,2″-terpyridyl)anthracene) is interesting in this context because it contains quinone ligands,[25−27] which may become redox noninnocent during catalysis to afford semiquinone and/or catecholate moieties. Consequently, the redox catalyst may access two spatially well-separated, chemically diverse storage sites for redox equivalents. In principle, distributing charges across a large molecular framework should be beneficial from energetic perspectives and allow for reducing unwanted radical-based reactivity. Prominent examples of chemical reactions where redox noninnocent ligands play a key role include catechol oxidase and galactose oxidase.[28−34] The chemistry of metal complexes with catechol/semiquinone ligands has been reviewed extensively by Pierpont and Lange.[35] More recently, the electronic structure of a

Received: December 5, 2010
Published: June 02, 2011

series of complexes with a single ruthenium center that engage in redox noninnocent behavior was investigated by Muckerman et al.[36,37] In unrelated previous work, we demonstrated that intimate coupling between the metal and the ligand redox states can play a significant role in determining the catalytic activity of a metal complex.[38,39]

The voltammetric response of the model complex $[Ru^{II}(trpy)(^tBu_2Q')(OH_2)]^{2+}$ (trpy = 2,2′:6′,2″-terpyridine, $^tBu_2Q'$ = 3,5-di-*tert*-butyl-1,2-benzoquinone) in electrochemical experiments suggested that deprotonation of the aqua ligand may lead to spontaneous intramolecular rearrangement of the electronic structure that transforms the quinone to semiquinone groups, as confirmed experimentally by low-temperature EPR studies.[26] By analogy, we may expect a similar response in the diruthenium catalyst complex upon deprotonation. An experimental complication arises from the fact that the catalyst is soluble in methanol but not in water. Hence, to study the reactivity of the catalyst in water it must be deposited on an ITO electrode surface and subsequently dipped in water. Interestingly, the aqueous UV−vis spectrum of the diruthenium species deposited on the electrode is similar to the spectrum of the species obtained after addition of two equivalents of ^{t}BuOK in methanol. This observation led to the conclusion that the catalyst may deprotonate spontaneously in water to afford a species matching the spectroscopic profile of the mononuclear analogue.[24] To form the O−O bond the two terminal oxo groups are expected to undergo intramolecular oxidation becoming oxyl radicals, while the removed electron is transported across the ruthenium conduit to the quinone ligands transforming them to semiquinone ligands. Having generated the two oxyl radical moieties facing each other, a radical recombination type of O−O coupling may ensue with little difficulty. Whereas this series of electronic rearrangement events is plausible, the required spontaneous deprotonation that triggers the series of transformations is surprising: In methanol the same reaction required the addition of the strong base ^{t}BuOK. *Why would this process be so much easier in water?* We investigated this tantalizing question in greater detail and reach a set of very different conclusions than proposed previously. A plethora of plausible redox and protonation states were probed systematically in an effort to obtain a robust foundation for drawing conclusions on the relative energetics and reactivities of the intermediates encountered in the redox series. Our calculations were calibrated against the experimentally observed reversible two-electron wave in cyclic voltammetry.[40] Recently, Muckerman et al. speculated on a mechanism where O−O bond formation is preceded by two proton-coupled electron transfer steps,[36] but a comprehensive and thorough quantum chemical treatment of the redox states of all plausible intermediates that we present here was thus far not available.

COMPUTATIONAL DETAILS

All calculations were carried out using density functional theory as implemented in the Jaguar 7.0 suite[41] of ab initio quantum chemistry programs. Geometry optimizations were performed with the B3LYP[42−46] functional and the 6-31G** basis set. Ru was represented using the Los Alamos LACVP basis[47,48] that includes relativistic effective core potentials. The energies of the optimized structures were re-evaluated by additional single-point calculations on each optimized geometry using Dunning's correlation-consistent triple-ζ basis set[49] cc-pVTZ(-f) that includes a double set of polarization functions. For Ru, we used a modified version of LACVP, designated as LACV3P, in which the exponents were decontracted to match the effective core potential with triple-ζ quality. Vibrational/rotational/translational entropies of the solute(s) were included using standard thermodynamic approximations. Solvation energies were evaluated by a self-consistent reaction field (SCRF)[50−52] approach based on accurate numerical solutions of the linearized Poisson−Boltzmann equation.[53] Solvation calculations were carried out at the optimized gas-phase geometry employing the dielectric constant of ε = 80.37 (water). As is the case for all continuum models, the solvation energies are subject to empirical parametrization of the atomic radii that are used to generate the solute surface. We employ the standard set of optimized radii for H (1.150 Å), C (1.900 Å), N (1.600 Å), and O (1.600 Å). The scaled van der Waals radius used for Ru is 1.481 Å. The solvation energies in methanol are computed using the dielectric constant of ε = 32.63. The probe radius is taken to be identical to that of water (1.4 Å). Tests using a larger probe radius (2.0 Å) show unsurprisingly a constant shift of the solvation energy not affecting the differential solvation energies to any relevant extent.

Convergence to plausible electronic states that correspond to conceptually meaningful electronic configurations was monitored by carefully observing the Mulliken spin densities and visualizing the frontier molecular orbitals. When multiple minima were encountered, we compared the total energies and chose the structure with the lowest energy. Antiferromagnetically (AF) coupled states were modeled using Noodleman's broken symmetry (BS) formalism without spin projection,[54−56] as the spin projection corrections are uniformly found to be negligibly small. Energy components have been computed following the protocol of our previous work.[40] The electron attachment free energy in solution phase $\Delta G^{EA}(sol)$ and the redox potentials ($E_{1/2}$) for the reactions were calculated as follows

$$\Delta G^{EA}(sol) = \Delta G^{EA}(gas) + \Delta\Delta G_{solv} \quad (1)$$

$$\Delta G^{EA}(gas) = \Delta H^{EA}(gas) - T\Delta S(gas) \quad (2)$$

$$\Delta H^{EA}(gas) = \Delta H^{EA}(SCF) + \Delta ZPE \quad (3)$$

$$\Delta G^{EA}(sol) = -nFE_{1/2} \quad (4)$$

where $\Delta G^{EA}(gas)$ = electron attachment free energy in the gas phase, $\Delta\Delta G_{solv}$ = free energy of solvation as computed using the continuum solvation model, $\Delta H^{EA}(gas)$ = electron attachment enthalpy in the gas phase, T = temperature (298.15 K), $\Delta S(gas)$ = entropy difference in the gas phase, $\Delta H^{EA}(SCF)$ = self-consistent field energy, i.e., "raw" electronic energy as computed from the SCF procedure, ΔZPE = vibrational zero-point energy difference, F = Faraday constant, and n = number of electrons. To correlate our computed redox potentials to experimental values that are reported against the Ag/AgCl reference electrode, we subtract 4.63 eV from the absolute potential that we obtain according to eq 4. The absolute potential of NHE is still debated with values ranging from 4.28 to 4.43 V.[57−61] Here, we assume the absolute potential of NHE to be 4.43 V, and thus, there may be a trivial systematic shift in our computed potentials up to 150 mV depending on which reference value is taken. For computing the proton-coupled redox reactions, it is necessary to account for the energy of a proton in solution. We used the following procedure to compute the free energy of a proton in solution, $G(H^+)$

$$G(H^+) = H^{gas}(H^+) - TS + 5/2RT + G_{solv}(H^+) \quad (5)$$

where $H^{gas}(H^+)$, the gas-phase electronic energy, is *zero* by definition, R is the universal gas constant, T is 298.15 K, S is the translational entropy of a free hydrogen atom (26.04 eu) calculated using the Sackur−Tetrode equation, and $G_{solv}(H^+)$ is the free energy of solvation (−265.9 kcal mol^{-1} in water and −263.9 kcal mol^{-1} in methanol).[62] At room temperature, the solution-phase free energy $G(H^+)$ is calculated to

dx.doi.org/10.1021/ic102427g |*Inorg. Chem.* 2011, 50, 5946–5957

be −11.80 eV in water and −11.72 eV in methanol. pK_a is calculated using the reaction isotherm

$$\Delta G(\text{sol}) = -RT \ln K_a = (2.303)RT\text{p}K_a = 1.36 \cdot \text{p}K_a \text{ (at 298.15 K)} \quad (6)$$

Our calculations are carried out on a slightly truncated model where the *tert*-butyl groups of the quinone ligands are replaced by hydrogen atoms (Figure 1). This smaller model system is validated by comparing calculated pK_as of the monoruthenium analogues mentioned in the text. The error we introduce by truncating the quinone ligand is limited to 1−2 pK_a units in this case.[63]

To clearly indicate the electronic structure of the intermediates, we use the following labels: For example, $[(\mathbf{x/q}),(\mathbf{y/sq})]^{2+}{}_{\text{OSS}}$ denotes the oxidation states of the ruthenium centers as x and y, respectively. The charge of the complex is 2+. The redox states of the ligands attached to Ru(x) and Ru(y) render the first to be a quinone, whereas the latter is characterized as a semiquinone ligand. The subscript denotes the open-shell singlet (OSS) electronic structure. The quinone is abbreviated as "q", while semiquinone, the one-electron-reduced form of quinone, is abbreviated as "sq". The metal oxidation states are assigned on the basis of Mulliken spin distribution and molecular orbital analysis.

RESULTS AND DISCUSSION

A key feature of any water oxidation mechanism that must be understood in detail is how and when the O−O bond is formed to afford typically a peroxo intermediate. In this case the reactant is assumed to be the dihydroxo complex $[(\mathbf{2/q}),(\mathbf{2/q})]^{2+}$. Tanaka proposed that this reaction is intimately connected to the deprotonation of $[(\mathbf{2/q}),(\mathbf{2/q})]^{2+}$ as summarized in Figure 2.[24] In methanol $[(\mathbf{2/q}),(\mathbf{2/q})]^{2+}$ displays a distinctive UV−vis absorption band at 580 nm, which is assigned to a $Ru^{II} \rightarrow$ quinone charge transfer (CT) transition. Upon addition of one equivalent of ^{t}BuOK, which presumably deprotonates $[(\mathbf{2/q}),(\mathbf{2/q})]^{2+}$, a new spectroscopic feature emerges at 850 nm that was assigned to a $Ru^{II} \rightarrow$ semiquinone CT transition. The presence of both the 580 and the 850 nm bands was considered to be a characteristic signature of the $[(\mathbf{2/q}),(\mathbf{2/sq})]^{+}$ cation, in which there is a $[(\text{quinone})Ru^{II}-OH]$ and a $[(\text{semiquinone})Ru^{II}-O^{\bullet}]$ moiety within one molecule giving rise to two distinct absorption bands. Removal of an additional H^+ by a second equivalent of ^{t}BuOK leads to a notably simplified UV−vis spectrum with only one absorption band at 850 nm. Thus, the intermediate $[(\mathbf{2/sq}),(\mathbf{2/sq})]^{0}$ was speculated to be a diruthenium peroxo complex with two $[(\text{semiquinone})Ru^{II}]$ centers bridged by a O−O fragment, as shown in Figure 2.[27] When $[(\mathbf{2/q}),(\mathbf{2/q})]^{2+}$ was exposed to water at pH = 4, the absorption band at 850 nm emerged spontaneously, leading to the interpretation that no external base is required for the complete deprotonation of $[(\mathbf{2/q}),(\mathbf{2/q})]^{2+}$ in water. This interpretation has significant mechanistic implications, as it implies that the overall two-electron oxidation of the hydroxo groups to the peroxo fragment is achieved spontaneously and rapidly under mild conditions only using two Ru^{II} promoter sites. If true, this finding is remarkable, as the oxo → peroxo conversion is often challenging and requires high-valent metal centers.[38] Second, the Ru^{II} centers do not formally change their oxidation states during the sequence of reactions in this mechanistic scenario, as the electrons that are formally removed from terminal oxo moiety are accommodated in the quinone ligands. Lastly, the spontaneous loss of two protons in water without the help of a strong base is puzzling since the pH of methanol is expected to be ∼7.3, i.e., notably higher than the pH of 4.0 used in aqueous solution, raising the question as to why the spontaneous deprotonation is not observed in methanol. In more recent work, the O−O bond formation was implicated to be preceded by two proton-coupled oxidations.[36] We examined the electronic structure and relative energies of the intermediates invoked in the mechanism to shed light on these tantalizing questions.

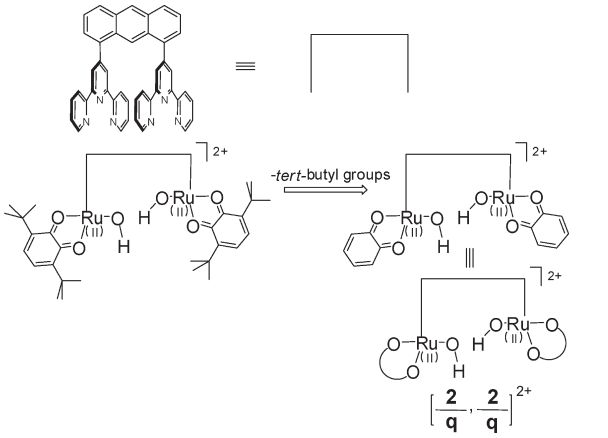

Figure 1. Computational model, and abbreviations used in this study.

Electronic Structure of $[2,2]^{2+}$. Before examining the energetics of the intermediates in various oxidation states it is necessary that we identify plausible electronic structures for all intermediates, most importantly for the starting point $[2,2]^{2+}$. With the metal centers and the quinone ligands potentially adopting different redox states a number of different electronic states are possible. On the basis of the 580 nm band Tanaka et al.[24] and subsequently Muckerman et al.[27] assigned the starting complex to be $[(\mathbf{2/q}),(\mathbf{2/q})]^{2+}$, i.e., two Ru^{II} centers supported by quinone ligands, which is the most intuitive assignment based on classical electron counting rules. We examined an extensive number of plausible alternative states in an effort to identify structural isomers and electronic features that may help explaining some of the questions highlighted above. To our surprise, we obtained two species that we labeled as $[(\mathbf{3/sq}),(\mathbf{3/sq})]^{2+}$ and $[(\mathbf{2/sq}),(\mathbf{3/sq})]^{2+}$ displaying significantly lower energies than $[(\mathbf{2/q}),(\mathbf{2/q})]^{2+}$ (Scheme 1).

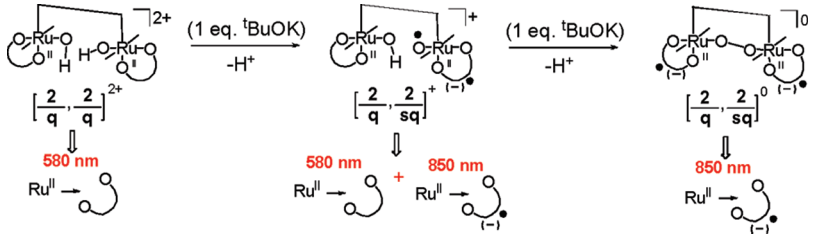

Figure 2. Tanaka's proposal for the deprotonation process in methanol in the presence of ^{t}BuOK.

dx.doi.org/10.1021/ic102427g |*Inorg. Chem.* 2011, 50, 5946–5957

Scheme 1

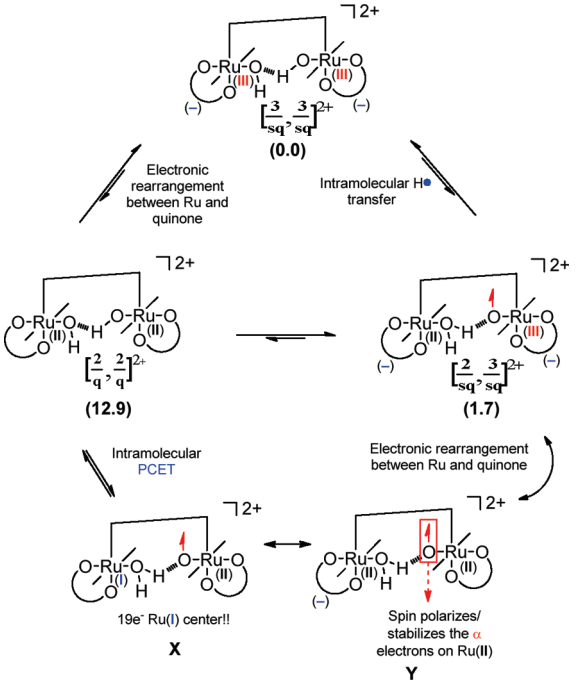

Their solution-phase free energies in water are 12.85 and 11.15 kcal mol^{-1} lower than that of $[(2/q),(2/q)]^{2+}$, respectively, indicating that the formally intuitive assignment of oxidation states is not appropriate in this case. Instead, there are two fairly isoenergetic forms constituting a better description of the nature of the key intermediate labeled as $[2,2]^{2+}$ thus far. Of these two alternative formulations $[(3/sq),(3/sq)]^{2+}$ is easy to understand, but the alternative $[(2/sq),(3/sq)]^{2+}$ requires some explanation.

Complex $[(3/sq),(3/sq)]^{2+}$ can be considered as the redox noninnocent analogue of $[2,2]^{2+}$, as it may be thought of as arising from the classical parent complex $[(2/q),(2/q)]^{2+}$ by formally inducing an intramolecular electron transfer across the Ru^{II}—quinone moiety to afford a Ru^{III}—semiquinone fragment where the unpaired electrons on Ru^{III}-d^5 and semiquinone centers are AF coupled. The Mulliken spin densities show significant excess α-spin density of 0.60 on Ru1 matched by an excess β-spin density of 0.85 on the quinone moiety Q1, which classifies the quinone group as a semiquinone. Similarly, the excess α-spin density of 0.61 on Ru2 is matched by a β-spin density of 0.76 on Q2 (Table 1, entry 3). This spin distribution is consistent with an intramolecular electron transfer from the Ru—O fragment to the quinone moiety directly bound to each of the metal centers. Since this species is computed to be the lowest energy structure, we use it as the reference state for all other isomers, as shown in Scheme 1.

Species $[(2/sq),(3/sq)]^{2+}$ can be derived from $[(2/q),(2/q)]^{2+}$ by H$^{\bullet}$ transfer from one hydroxo unit to the other hydroxo group of the molecule, leaving behind an unpaired electron on the resulting terminal oxyl moiety, as illustrated in Scheme 1. The Mulliken spin densities of 0.97 and −0.12, i.e., an excess α-population of 0.97 and an excess β-population of 0.12 on Ru1 and Ru2, respectively, are fully consistent with a Ru^{III}-d^5 and Ru^{II}-d^6 center, respectively. We can envision this new electronic structure to arise from the following series of formal transformations. First, we imagine invoking an intramolecular proton-coupled electron transfer (PCET) to afford a conceptual intermediate complex **X**. The hydrogen-bonded hydroxo groups of the Ru2—(OH)···(HO)—Ru1 moiety become a Ru2—(O H$_2$)···(O)—Ru1 fragment in this process, as illustrated in Scheme 1. This process affords an energetically undesirable 19-electron Ru^{I} center that is attached to the newly formed aqua ligand in intermediate **X**. This electronic stress can be released, if the electron is moved further to the quinone ligand, which generates a (semiquinone)—Ru^{II}—(OH$_2$) fragment in the conceptual intermediate **Y**. Concomitantly, the drastic change in the Coulombic and electronic character of the oxyl radical bound to Ru1 compared to the hydroxo ligand triggers the metal to donate a β-electron to the quinone ligand that is directly attached to it, giving a semiquinone on both sides of the diruthenium complex in $[(2/sq),(3/sq)]^{2+}$. The most salient structural features of these three isomers are shown in Figure 3. The hydrogen-bonding patterns are in good agreement with the electronic patterns described above and will not be discussed in greater detail.

Table 1. Mulliken Spin Density Distributions of Various Structures Encountered during the Deprotonation Series[a]

	Ru2	O2	Q2	tpy2	Ru1	O1	Q1	tpy1
$[(2/q),(2/q)]^{2+}$	0.00	0.00	0.00	0.00	0.00	0.00	0.00	0.00
$[(2/sq),(3/sq)]^{2+}$	−0.12	0.01	−0.89	0.01	0.97	0.87	−0.88	0.03
$[(3/sq),(3/sq)]^{2+}$	0.61	0.16	−0.76	−0.01	0.60	0.27	−0.85	−0.01
$[(2.5/sq),(2.5/sq)]^{+}$	0.51	0.36	−0.89	−0.01	0.56	0.64	−0.91	−0.24
$[(2.5/sq),(2.5/sq)]^{0}$	0.69	0.82	−0.91	−0.56	0.69	0.82	−0.91	−0.57
$^{a}[(2.5/sq),(2.5/sq)]^{0}$	0.68	0.80	−0.90	−0.55	−0.68	−0.80	0.90	0.55
$[(2/sq),(2/sq)]^{0}_{OSS}$	0.29	0.12	0.68	−0.18	−0.21	0.03	−0.75	0.02
$[(2/sq),(2/sq)]^{0}_{T}$	0.23	0.22	0.67	−0.12	0.29	0.27	0.60	−0.15

[a] Positive numbers indicate α-spin, and negative numbers indicate β-electron density.

The different contributions to the solution-phase free energy of the three species are compared in Table 2. Interestingly, the energetic preference of $[(3/sq),(3/sq)]^{2+}$ over $[(2/q),(2/q)]^{2+}$ is dominated by an electronic energy difference of 12.1 kcal mol^{-1} in favor of $[(3/sq),(3/sq)]^{2+}$. All other components of the solution-phase free energy are practically identical for both complexes. It is particularly meaningful that the solvation energies of these two species are identical at −111.4 kcal mol^{-1} in methanol and −113.9 kcal mol^{-1} in water. Thus, the energetic preference of $[(3/sq),(3/sq)]^{2+}$ over $[(2/q),(2/q)]^{2+}$ is an intrinsic feature of the catalyst that stems from the redox noninnocent nature of the quinone ligand in $[(3/sq),(3/sq)]^{2+}$. The alternative species $[(2/sq),(3/sq)]^{2+}$ is *electronically* only 4.0 kcal mol^{-1} lower in energy than the classical "redox innocent" parent complex $[(2/q),(2/q)]^{2+}$. However, it shows a significantly more polarized electron density distribution than the parent, which is easy to understand given the electronic and structural rearrangement discussed above. The dipole moment of $[(2/sq),(3/sq)]^{2+}$ is 8.7 D, which is much larger than 3.4 D in $[(2/q),(2/q)]^{2+}$. Consequently, the solvation energy of $[(2/sq),(3/sq)]^{2+}$ is 6 kcal mol^{-1} more negative than that of $[(2/q),(2/q)]^{2+}$ (Table 3).

The energy component analysis presented above leads to an important conclusion. If taken without the proper skepticism for the accuracy of the computed numbers, we may conclude that $[(3/sq),(3/sq)]^{2+}$ is the dominant species in both water and methanol, since it has the lowest energy in both solvents. We have to consider, however, that our continuum model is a very simplistic treatment of the solvation effect at best. What are more meaningful than the absolute magnitudes of the calculated solvation energies are the underlying electronic features that

dx.doi.org/10.1021/ic102427g |*Inorg. Chem.* 2011, 50, 5946–5957

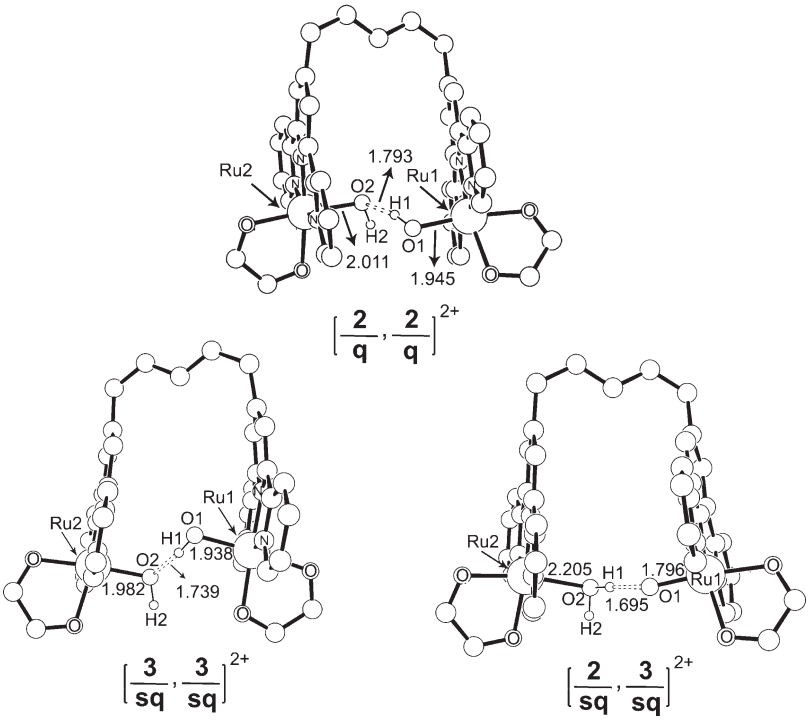

Figure 3. Structures of the alternative candidates for the ground electronic state of $[\mathbf{2,2}]^{2+}$. Only the core structures are shown for clarity; only a few selected carbon atoms of the anthracene and the quinone fragments are drawn, and all nonessential hydrogen atoms are hidden.

Table 2. Relative Energetics of the Different Electronic and Structural Isomers of $[\mathbf{2,2}]^{2+}$

		ΔG(solv.)		ΔG(sol)	
	ΔE(SCF)	water	methanol	water	methanol
$[\mathbf{(2/q),(2/q)}]^{2+}$	0.00	−113.93	−111.40	0.00	0.00
$[\mathbf{(3/sq),(3/sq)}]^{2+}$	−12.13	−113.92	−111.35	−12.85	−12.81
$[\mathbf{(2/sq),(3/sq)}]^{2+}$	−3.97	−119.89	−117.20	−11.15	−10.99

Table 3. Mulliken Spin Density Distributions of Various Structures Encountered during the Deprotonation Series[a]

	Ru2	O2	Q2	tpy2	Ru1	O1	Q1	tpy1
$[\mathbf{(2/q),(2/q)}]^{2+}$	0.00	0.00	0.00	0.00	0.00	0.00	0.00	0.00
$[\mathbf{(2/sq),(3/sq)}]^{2+}$	−0.12	0.01	−0.89	0.01	0.97	0.87	−0.88	0.03
$[\mathbf{(3/sq),(3/sq)}]^{2+}$	0.61	0.16	−0.76	−0.01	0.60	0.27	−0.85	−0.01
$[\mathbf{(2.5/sq),(2.5/sq)}]^{+}$	0.51	0.36	−0.89	−0.01	0.56	0.64	−0.91	−0.24
$[\mathbf{(2.5/sq),(2.5/sq)}]^{0}$	0.69	0.82	−0.91	−0.56	0.69	0.82	−0.91	−0.57
[a] $[\mathbf{(2.5/sq),(2.5/sq)}]^{0}$	0.68	0.80	−0.90	−0.55	−0.68	−0.80	0.90	0.55
$[\mathbf{(2/sq),(2/sq)}]^{0}_{OSS}$	0.29	0.12	0.68	−0.18	−0.21	0.03	−0.75	0.02
$[\mathbf{(2/sq),(2/sq)}]^{0}_{T}$	0.23	0.22	0.67	−0.12	0.29	0.27	0.60	−0.15

[a] Positive numbers indicate α-spin, and negative numbers indicate β-electron density.

led to the energy difference. In addition, the computed energy difference of 1.8 kcal mol^{-1} in favor of $[\mathbf{(3/sq),(3/sq)}]^{2+}$ over $[\mathbf{(2/sq),(3/sq)}]^{2+}$ is too small to allow for a confident decision on $[\mathbf{(3/sq),(3/sq)}]^{2+}$ being the dominant form. Taken together these results present an elegant albeit speculative proposal for explaining the tantalizing spectroscopic observations mentioned above: In methanol the dominant intermediate is the electronically most favorable species $[\mathbf{(3/sq),(3/sq)}]^{2+}$, whereas $[\mathbf{(2/sq),(3/sq)}]^{2+}$ is dominant in water. Previous work by Tsai et al.[64] is interesting in this context, as it showed that a $Ru^{II}-O^{\bullet}$ moiety of the mononuclear model complex abstracts an H atom presumably from CF_3CH_2OH at room temperature to afford the hydroxo analogue. By analogy we may expect $[\mathbf{(2/sq),(3/sq)}]^{2+}$ to engage in a similar reaction. On closer inspection, however, we note distinctive differences between the mononuclear model and this dinuclear catalyst: (i) In $[\mathbf{(2/sq),(3/sq)}]^{2+}$ the oxyl radical is masked by strong H bonding to the aqua ligand of the other Ru subunit. (ii) The $Ru^{III}-O^{\bullet}$ moiety in $[\mathbf{(2/sq),(3/sq)}]^{2+}$ is expected to be much less likely to engage in a H-atom abstraction reaction, as the unpaired spin on the Ru^{III}-d^5 center will stabilize the oxyl radical more effectively. Calculations on the model mononuclear complex $[\mathbf{(3/sq)}]^{+}$ confirm that the H-atom transfer reaction is ∼10 kcal mol^{-1} more uphill than for the $[\mathbf{(2/sq)}]^{0}$ species. (iii) The mononuclear oxyl radical model complex is neutral, whereas the corresponding subunit in the dinuclear complex is positively charged, making the latter less susceptible to protonation in acidic pH. The presence of $[\mathbf{(2/sq),(3/sq)}]^{2+}$ in water provides a plausible explanation as to why a more flexible bridge like 2,7-di-*tert*-butyl-9,9-dimethyl-4,5-bis(2,2′:6′,2″-terpyrid-4′-yl)-xanthene may lead to an unreactive bridging oxo complex,[27] as it is easy to envision that the extrusion of the preformed water ligand will lead to formation of the Ru−O−Ru moiety.

Deprotonation. Previously, the spectroscopically detectable species were identified to be $[\mathbf{(2/q),(2/q)}]^{2+}$, $[\mathbf{(2/q),(2/sq)}]^{+}$, and $[\mathbf{(2/sq),(2/sq)}]^{0}$ assuming that the hydroxo ligands are sufficiently acidic to lose the protons under the experimental conditions. As our new proposal deviates significantly from this original assignment, we must critically evaluate the deprotonation events specifically to highlight and rationalize the differences.

dx.doi.org/10.1021/ic102427g |*Inorg. Chem.* 2011, 50, 5946–5957

The rationale for expecting the hydroxo groups to be fairly acidic stems from comparing them to the analogous species $[Ru^{II}(tpy)(^tBu_2Q')(OH_2)]^{2+}$, for which a p$K_a$ of 5.5 was reported in water.[26] This comparison is problematic, however, as the acidic proton originates from an aqua ligand in this case and progresses according to $(q)Ru^{II}-OH_2 \rightarrow (q)Ru^{II}-OH + H^+$, whereas in $[(3/sq),(3/sq)]^{2+}$ the deprotonation involves $(sq)Ru^{III}-OH \rightarrow (sq)Ru^{III}-O^- + H^+$, as summarized in Scheme 2. On the basis of the fact that the hydroxo is expected to be much less acidic than the aqua ligand we may expect the latter to be much less acidic than $[Ru^{II}(tpy)(^tBu_2Q')(OH_2)]^{2+}$. On the other hand, the presence of the Ru^{III} center in $[(3/sq),(3/sq)]^{2+}$ may contribute to increasing the acidity. In any case, it is clear that $[Ru^{II}(tpy)(^tBu_2Q')(OH_2)]^{2+}$ is not a good model complex from which to derive estimates for the pK_a values of the diruthenium complex given the unexpectedly complex electronic structure. For $[(2/sq),(3/sq)]^{2+}$, our proposed dominant species in water, the deprotonation event appears more comparable to the monometallic analogue, as the acidic proton originates from an aqua ligand bound to Ru^{II}. The charge of the corresponding subunit is formally 1+, however, and we expect the acidity to be decreased significantly as a result. Another obvious difference is that there are two protons within the same molecule, and it is likely that they will influence each other, leading to two substantially different pK_a's for the two potentially acidic protons.

Scheme 2

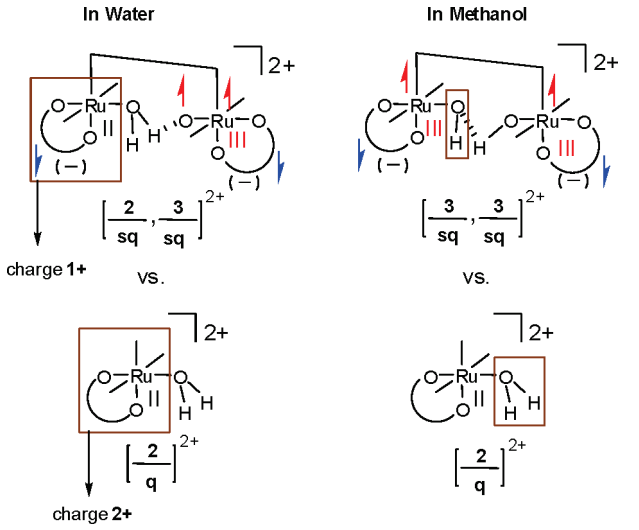

In Methanol. Figure 4 shows our proposed sequence of proton removal in methanol. As expected, there is a strong intramolecular hydrogen bond between the two hydroxo moieties in $[(3/sq),(3/sq)]^{2+}$ with a O2···H1 distance of 1.739 Å connecting the two ruthenium centers. Consequently, the first proton to be removed is H2, which is not involved in the intramolecular hydrogen bonding, and our calculations predict a pK_a1 of 22.6 for this process based on a solution-phase free energy change of 30.8 kcal mol^{-1}. Our calculations indicate significant spin polarizations in this deprotonation intermediate with the excess of α-spin densities at Ru2 and Ru1 reaching 0.51 and 0.56, respectively (Table 1, entry 4). The oxygen atoms of the

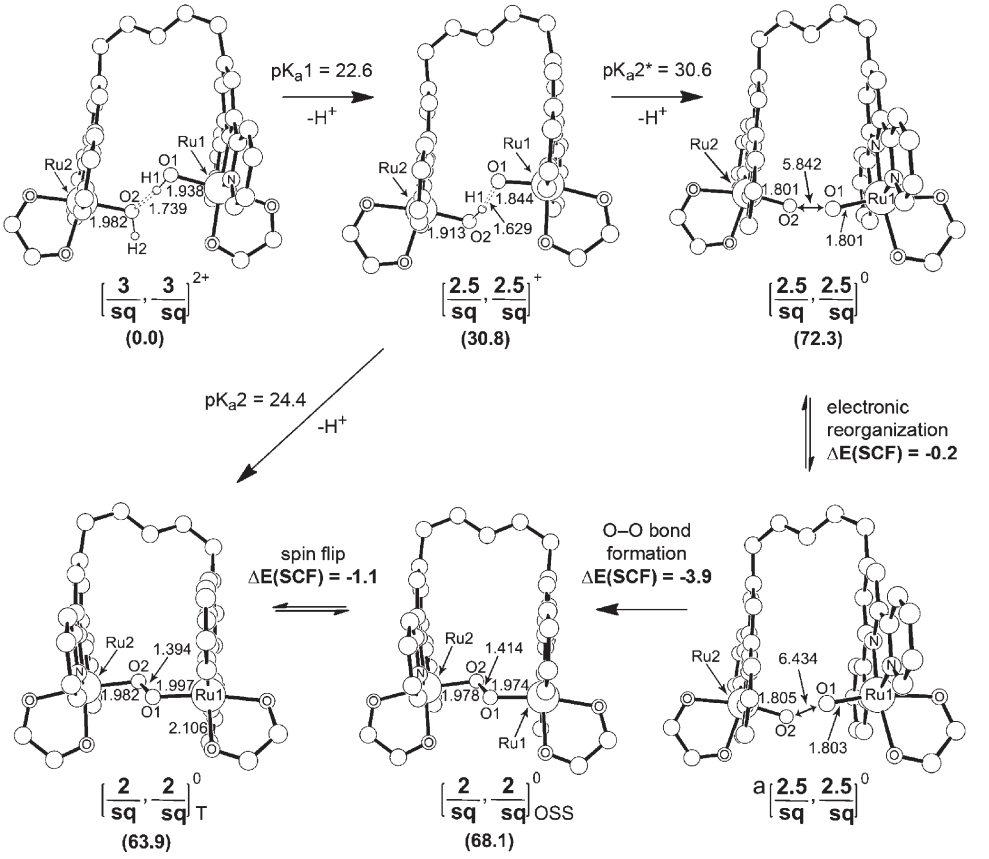

Figure 4. Structures of the intermediates during the deprotonation process in methanol. Solution-phase free energies in kcal mol^{-1} are given in parentheses. Electronic energy differences ΔE(SCF) are also in kcal mol^{-1}.

dx.doi.org/10.1021/ic102427g |*Inorg. Chem.* 2011, 50, 5946–5957

Scheme 3

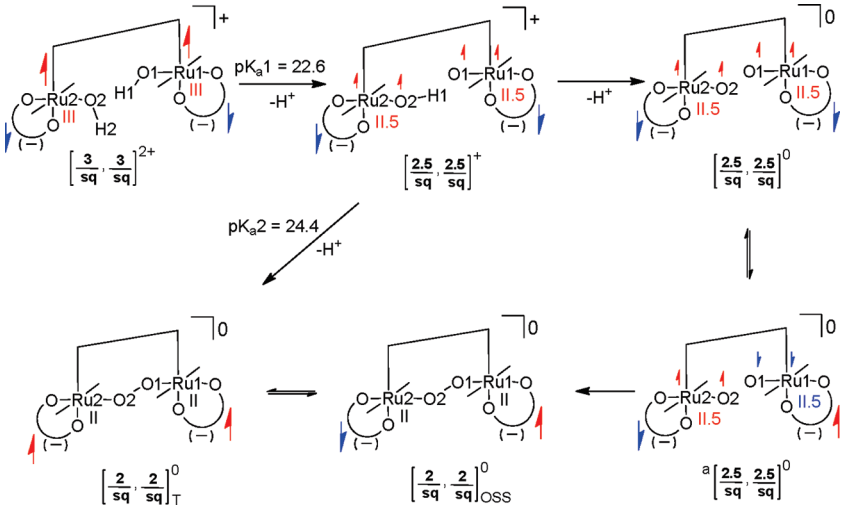

hydroxo/oxo groups accommodate α-spin densities of 0.36 and 0.64 on O2 and O1, respectively. The corresponding β-electron density is found on the quinone moieties with 0.89 and 0.91 equivalents of unpaired β-electrons being located on them, respectively. This spin distribution is consistent with the electronic structure of two Ru centers formally in oxidation states of +2.5 flanked by semiquinone ligands each accommodating one unpaired electron (Scheme 3). Thus, we label this complex as $[(\mathbf{2.5/sq}),(\mathbf{2.5/sq})]^{+}$ in Figure 4.

Removing the second proton is even more difficult with a predicted conceptual pK_a2* of 30.6 (Figure 4), which is in good agreement with our intuitive expectation that removal of the second proton from the overall cationic complex should be energetically more demanding than removing the first proton from the dicationic system. The intramolecular hydrogen bond is also expected to contribute significantly to increasing the pK_a. Electronically, removal of the positive charge located between the two oxygen atoms triggers additional β-electron transfer from the oxygen to the metal fragment, thereby increasing the unpaired α-electron density on O1 from 0.64 to 0.82. Interestingly, the additional β-electron density is directly dissipated from the metal to the tpy ligand, allowing the Ru center to maintain its oxidation state at 2.5. Therefore, this species is labeled as $[(\mathbf{2.5/sq}),(\mathbf{2.5/sq})]^{0}$ in Figure 4. Realistically, the O−O bond formation will take place after the deprotonation event, as the two terminal oxyl radical groups in $[(\mathbf{2.5/sq}),(\mathbf{2.5/sq})]^{0}$ should couple easily. To do so, intermediate $[(\mathbf{2.5/sq}),(\mathbf{2.5/sq})]^{0}$ must first invert the spins located on one of the metal fragments relative to the other metal fragment, as to place unpaired electrons with opposite spins on each of the terminal oxyl groups. This process is expected to be easy, as the two subunits are connected by a considerably large spacer, and hence, the electronic communication is negligible. Consistent with this reasoning is that our calculations indicate that species $^{a}[(\mathbf{2.5/sq}),(\mathbf{2.5/sq})]^{0}$ is practically isoenergetic with $[(\mathbf{2.5/sq}),(\mathbf{2.5/sq})]^{0}$ and the O−O bond can be formed readily with an electronic driving force of 4 kcal mol^{-1} to give a peroxo species in which two unpaired electrons reside on the two semiquinone ligands. As we expect negligible electronic communication between the two semiquinone moieties, the triplet analogue $[(\mathbf{2/sq}),(\mathbf{2/sq})]^{0}_{T}$ is anticipated and confirmed to be nearly isoenergetic with a ΔE(SCF) of −1.1 kcal mol^{-1}. Thus, the final product of the second deprotonation and O−O bond formation is the triplet complex $[(\mathbf{2/sq}),(\mathbf{2/sq})]^{0}_{T}$, which results in a p$K_a$2 of 24.4 that we propose to correlate to the experimentally observable second deprotonation. The O−O bond formation stabilizes the doubly deprotonated product significantly and allows one to decrease the second pK_a notably compared to pK_a2*. As a consequence the two pK_a values are very close to each other at 22.6 and 24.4 and are comparable to the pK_a of ^{t}BuOH in methanol, which can be estimated to be ∼21.[65] Hence, our calculations fully support Tanaka's original proposal that addition of ^{t}BuOK to a solution of $[(\mathbf{3/sq}),(\mathbf{3/sq})]^{2+}$ in methanol deprotonates the hydroxo groups and triggers O−O bond formation.

Tanaka rationalized the observation of both 580 and 850 nm bands in the UV−vis spectrum upon addition of one equivalent of ^{t}BuOK by invoking the presence of $[(\mathbf{2/q}),(\mathbf{2/sq})]^{+}$ species that contains both Ru^{II}−quinone and Ru^{II}−semiquinone moieties. In our calculations, deprotonation leads to the formation of semiquinone in both the subunits.[66] This apparent disagreement between the experimentally observed spectra and the calculated structures can be resolved if we consider that pK_a values of the two acidic protons are almost identical and very close to the pK_a of ^{t}BuOH (∼21), suggesting that both the singly deprotonated and the fully deprotonated species will be present in equilibrium during the deprotonation process. If we tentatively assign the 580 nm band to $[(\mathbf{3/sq}),(\mathbf{3/sq})]^{2+}$ and the 850 nm band to $[(\mathbf{2.5/sq}),(\mathbf{2.5/sq})]^{+}$ and $[(\mathbf{2/sq}),(\mathbf{2/sq})]^{0}_{T}$, the observed UV−vis spectrum upon addition of the first and second equivalents of ^{t}BuOK can be explained as follows. During the removal of the first proton the fully protonated species $[(\mathbf{3/sq}),(\mathbf{3/sq})]^{2+}$ is present and affords an absorption band of 580 nm while the singly deprotonated species $[(\mathbf{2.5/sq}),(\mathbf{2.5/sq})]^{+}$ has an absorption band at 850 nm. When the second proton is removed, only $[(\mathbf{2.5/sq}),(\mathbf{2.5/sq})]^{+}$ and the fully deprotonated species $[(\mathbf{2/sq}),(\mathbf{2/sq})]^{0}_{T}$ are present and exhibit an absorption band around 850 nm. Although the above proposal seems to be plausible, it remains a speculation since the absorption spectra of these complexes cannot be computed reliably, as the open-shell nature and the broken symmetry orbitals we utilize to approximate the intrinsically multiconfigurational electronic structure within the DFT framework make it impossible to properly compute the

dx.doi.org/10.1021/ic102427g |*Inorg. Chem.* 2011, 50, 5946–5957

response properties, which are required to calculate the optical transitions within the time-dependent DFT formalism. Despite these fundamental concerns, we attempted to calculate the absorption spectra of these intermediate species with TDDFT and confirmed that the results are not sensible. Some of these results are discussed in the Supporting Information for completeness.

In Water. The deprotonation of $[(\mathbf{2/sq}),(\mathbf{3/sq})]^{2+}$ was initially proposed to be spontaneous in water. In our calculations the first deprotonation leads to species $[(\mathbf{2.5/sq}),(\mathbf{2.5/sq})]^{+}$ where 2α-spin density is distributed across the molecular structure as depicted in Scheme 4. The change in free energy for this process in water is calculated to be 28.0 kcal mol^{-1}, which corresponds to a pK_a of 20.6, much too high to justify spontaneous deprotonation in water at pH 4. Tanaka's proposal was partly derived from the observation that the mononuclear analogue $[(\mathbf{2/q})]^{2+}$ displays a pK_a of 5.5,[64] and our calculations reproduce this experimental observation well with a calculated pK_a of 6.1 (Table 4 and Scheme 4). Whereas this analogy is plausible in the sense that both species are dications and the acidic protons originate from a water ligand, our calculations suggest that this comparison is flawed because in $[(\mathbf{2/sq}),(\mathbf{3/sq})]^{2+}$ there are (sq)Ru^{II}−OH$_2$ and (sq)Ru^{III}−O$^{\bullet}$ fragments with the positive charges distributed over these two metal sites. Hence, deprotonation of the aqua ligand is electrostatically much more difficult in the dinuclear species compared to the mononuclear analogue $[(\mathbf{2/q})]^{2+}$, as confirmed in the electronic energy requirement of 239.4 kcal mol^{-1} compared to 191.7 kcal mol^{-1}, respectively. Addition of differential solvation energy and entropy results in a final energy difference of 28 vs 8 kcal mol^{-1} (Table 4). Figure 5 summarizes the differences between our proposal and what was suggested by Tanaka previously. There is agreement that deprotonation of the diruthenium complex in methanol by two equivalents of ^{t}BuOK leads to formation of an O−O bond. Spontaneous deprotonation in water, however, is found to be implausible energetically. Moreover, the electronic structure of the parent molecule is consistent with a Ru^{III}−(sq) representation rather than Ru^{II}−(q).

Scheme 4

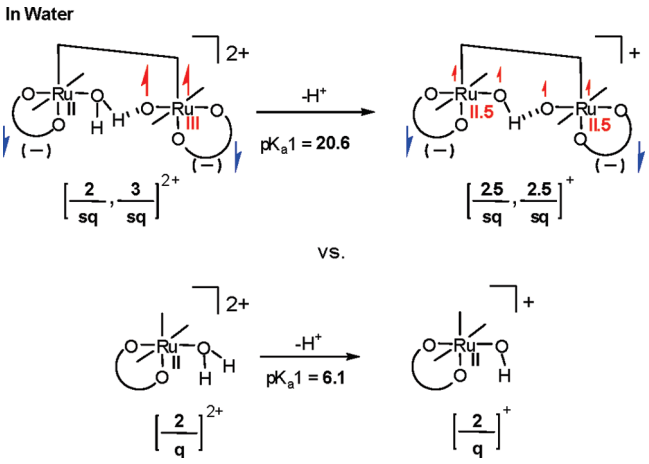

Electrochemical Oxidation. Whereas the deprotonation events and the ensuing O−O bond formation provided important insight into the electronic structure of the Tanaka catalyst, the catalytic reaction is driven by electrochemical oxidation without the involvement of a strong base. Therefore, we investigated the electrochemical redox steps in an attempt to identify the various redox intermediates that must be traversed to form the final catalytically active species. Experimentally, a broad redox wave is observed around 0.32 V vs Ag/AgCl, followed by an irreversible wave at 1.19 V and a catalytic current at ∼1.5 V where water oxidation takes place. We began our redox series with complex $[(\mathbf{2/sq}),(\mathbf{3/sq})]^{2+}$, which we proposed to be the most probable resting state complex in water (vide supra). This complex adopts an open-shell singlet configuration with an identical number of electrons in the α- and β-spin domains. Ru2, which carries the aqua ligand, is in a low-spin Ru^{II}-d^6 configuration reflected in only a slight overpopulation of β-spin density 0.12 with the semiquinone ligand accommodating a full equivalent of one unpaired β-electron, as discussed above (Table 1, entry 2). The other ruthenium center carries an oxyl radical ligand with an α-electron excess of 0.87, consistent with a Ru^{III}-d^5 low-spin configuration, and exposes approximately one full unpaired α-spin electron with a Mulliken spin density of 0.97. Given the discussion of the electronic structure presented above, it is not surprising that the redox-active orbitals, the highest occupied spin orbital (HOSO) and lowest unoccupied spin orbital (LUSO), are ligand based and centered on the semiquinone groups. The HOSO of $[(\mathbf{2/sq}),(\mathbf{3/sq})]^{2+}$, illustrated in Figure 6, is located on the semiquinone bound to Ru2 with an

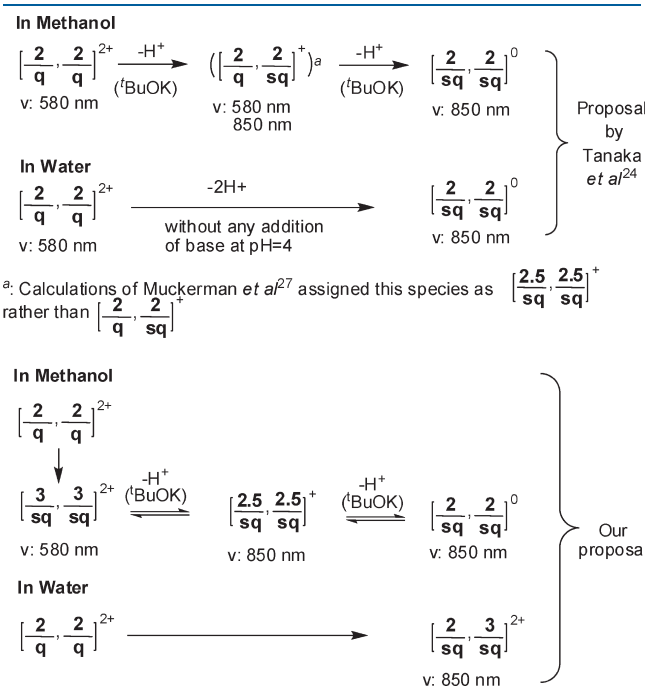

Figure 5. Similarities and contrasts between our current hypothesis and the one originally proposed by Tanaka and Muckerman et al.[24,27]

Table 4. Comparison of the First pK_a of the Diruthenium Complex with the Monometallic Model Complex

	ΔE(SCF)	ΔΔG_{solv}	ΔG(sol)	pK_a
$[(\mathbf{2/sq}),(\mathbf{3/sq})]^{2+} \rightarrow [(\mathbf{2.5/sq}),(\mathbf{2.5/sq})]^{+} + H^{+}$	239.44	−197.16	27.97	20.57
$[(\mathbf{2/q})]^{2+} \rightarrow [(\mathbf{2/q})]^{+} + H^{+}$	191.70	−171.00	8.34	6.14

dx.doi.org/10.1021/ic102427g |*Inorg. Chem.* 2011, 50, 5946–5957

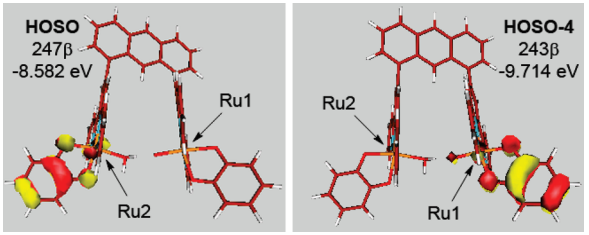

Figure 6. Isodensity plots (isodensity value = 0.05 au) of the occupied orbitals accommodating the unpaired β-electron spin on the semiquinone ligands.

orbital energy of −8.582 eV. The corresponding orbital on the other semiquinone moiety is HOSO−4 at −9.714 eV. These notable energy differences are interesting, as they allow for gauging the influence of the electronic structure of the two Ru−O fragments on the energies of the redox noninnocent semiquinone ligands. Formally, both Ru fragments $(sq)Ru2^{II}-OH_2$ and $(sq)Ru1^{III}-O^{\bullet}$ have an overall charge of 1+, but Ru1 is formally in a +III oxidation state, thus exerting a much stronger positive electrostatic potential on the ligands bound to it than Ru2, which is formally in a +II oxidation state. Consequently, all occupied orbitals on the Ru1 side of the complex are expected to be lower in energy, as highlighted by the two semiquinone radical orbitals shown in Figure 6. This electronic structure has a profound impact on the redox activity of diruthenium complex rendering one-half of the molecule that contains the Ru1 fragment inactive for the first two oxidation events.

Removal of the first electron from $[(\mathbf{2/sq}),(\mathbf{3/sq})]^{2+}$ gives $[(\mathbf{2/q}),(\mathbf{3/sq})]^{3+}$ where the electron originates from the semiquinone moiety bound to the Ru2 center to afford a quinone−Ru2 moiety leaving the electronic structure of the Ru1 subunit unchanged (step Ia in Scheme 5). This finding is consistent with the HOSO being mostly located on the Ru2−seminquinone fragment, as described above. The Mulliken spin density difference between $[(\mathbf{2/sq}),(\mathbf{3/sq})]^{2+}$ and $[(\mathbf{2/q}),(\mathbf{3/sq})]^{3+}$ supports our assignment that the redox-active electron originates from the semiquinone moiety, as the only significant change is found to be β-spin density reduction of the Q2 fragment from 0.89 to 0.08 (Table 1, entry 1 and Table 5, . entry 1). Not surprisingly, this oxidation event increases the acidity of the aqua ligand bound to Ru2 significantly. Our calculations suggest a pK_a of 3.9 and therefore predict that $[(\mathbf{2/q}),(\mathbf{3/sq})]^{3+}$ will deprotonate readily under the experimental conditions at pH 4 (step Ib in Scheme 5). Removal of the proton generates a hard hydroxo ligand bound to the soft Ru^{II} center, which is energetically not favorable. This mismatched M−L pairing can be alleviated by transferring one valence electron from the Ru^{II} center to the quinone ligand to afford a Ru^{III}−semiquinone intermediate $^{a}[(\mathbf{3/sq}),(\mathbf{3/sq})]^{2+}_{D}$, where the subscript D denotes the doublet spin state. This sequence of proton-coupled electron transfer is nonclassical, as we typically expected the transition metal center to be the redox-active site. Overall, the first proton-coupled oxidation transforms a $Ru^{II}-(sq)$ to a $Ru^{III}-(sq)$ moiety, labeled as step I in Scheme 5, and is associated with a redox potential of 0.436 V vs Ag/AgCl. Our calculations indicate, however, that this oxidation is mediated by the redox-active semiquinone/quinone ligand, which serves as a redox conduit utilizing the proton to formally trigger intramolecular electron transfer across the Ru−(q/sq) fragment. Whereas this mechanistic detail does not change the overall thermodynamics of the proton-coupled oxidation originating from the $Ru^{II}-(sq)/Ru^{III}-(sq)$ pair, it will provide a distinctive advantage for the electron transfer kinetics and electron transfer efficiency likely reducing the overpotential associated with this oxidation process and will thereby increase the versatility of the catalyst. From a rational catalyst design perspective, this insight is interesting because it assigns a clear function to the redox noninnocent quinone ligands.

The unusual utilization of the semiquinone fragment as a redox conduit creates an intriguing electronic scenario for the second oxidation. The highest occupied spin orbital of $^{a}[(\mathbf{3/sq}),(\mathbf{3/sq})]^{2+}_{D}$, the intermediate product of the first oxidation, is

Scheme 5

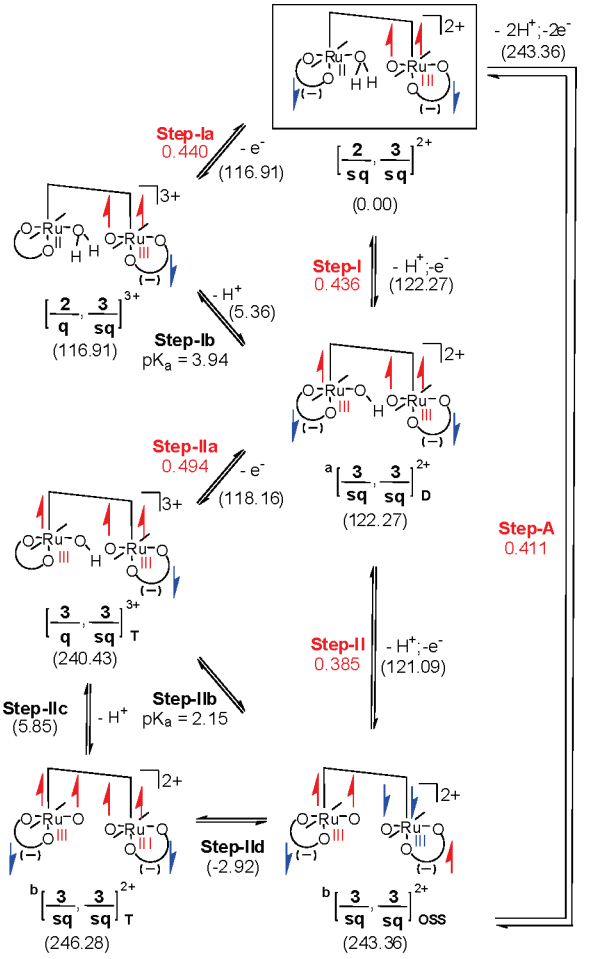

Table 5. Mulliken Spin Densities on the Key Atoms of the Various Redox States

	Ru2	O2	Q2	tpy2	Ru1	O1	Q1	tpy1
$[(\mathbf{2/q}),(\mathbf{3/sq})]^{3+}$	0.08	0.01	−0.08	0.00	1.01	0.80	−0.84	0.01
$^{a}[(\mathbf{3/sq}),(\mathbf{3/sq})]^{2+}_{D}$	0.59	0.26	−0.83	0.00	0.92	0.91	−0.89	0.04
$[(\mathbf{3/q}),(\mathbf{3/sq})]^{3+}_{T}$	0.71	0.34	−0.22	0.00	0.97	0.85	−0.72	0.04
$^{b}[(\mathbf{3/sq}),(\mathbf{3/sq})]^{2+}_{T}$	0.88	0.98	−0.91	0.05	0.89	0.98	−0.91	0.04
$^{b}[(\mathbf{3/sq}),(\mathbf{3/sq})]^{2+}_{OSS}$	−0.88	−0.98	0.90	−0.03	0.88	0.98	−0.91	0.05

dx.doi.org/10.1021/ic102427g |Inorg. Chem. 2011, 50, 5946–5957

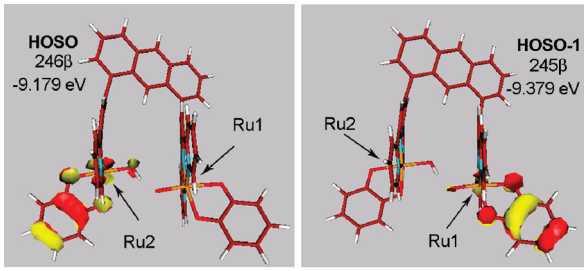

Figure 7. Isodensity plots (isodensity value = 0.05 au) of the occupied orbitals accommodating the unpaired β-electron spin on the semiquinone ligands.

practically identical to that of the fully reduced species $[(\mathbf{2/sq}),(\mathbf{3/sq})]^{2+}$, as a visual inspection of the HOSOs shown in Figures 6 and 7 demonstrates. It is mostly located on the semiquinone unit bound to Ru2 with an orbital energy of −9.179 eV. Interestingly, removal of the redox-active electron, step IIa in Scheme 5, requires 0.494 V vs Ag/AgCl, which is strikingly close to 0.440 V computed for the first oxidation. Similarly, the pK_a of the hydroxo group bound to Ru2 is calculated to be 2.15, which is also close to the pK_a of 3.94 associated with the loss of a proton in the first oxidation step. Consequently, we propose that the second deprotonation is also spontaneous at the experimental condition (step IIb in Scheme 5) to afford the open-shell singlet complex ${}^{b}[(\mathbf{3/sq}),(\mathbf{3/sq})]^{2+}_{OSS}$. A slight complication compared to the first oxidation process arises as intersystem crossing from the triplet state to the open-shell singlet surface takes place upon proton-coupled electron transfer. As shown in step IIc of Scheme 5, deprotonation of $[(\mathbf{3/q}),(\mathbf{3/sq})]^{3+}_{T}$ gives rise to ${}^{b}[(\mathbf{3/sq}),(\mathbf{3/sq})]^{2+}_{OSS}$, which displays symmetric spin distributions across the (sq)−[Ru−O] fragments in both halves of the complex. We found that inversion of the unpaired spins on one side of the molecule to generate the open-shell singlet analogue ${}^{b}[(\mathbf{3/sq}),(\mathbf{3/sq})]^{2+}_{OSS}$ (step IId) is energetically favorable by 2.92 kcal mol^{-1}. The computed Mulliken spin densities allow again for identifying the semiquinone/quinone ligand Q2 to be the redox conduit with the spin densities indicating a reduction of excess β-spin density from 0.83 to 0.22 for the oxidation step ${}^{a}[(\mathbf{3/sq}),(\mathbf{3/sq})]^{2+}_{D} \rightarrow [(\mathbf{3/q}),(\mathbf{3/sq})]^{3+}_{T}$. As seen before, deprotonation leads to excess electron density at the Ru−O moiety, which is dissipated by intramolecular electron transfer to the quinone ligand, as outlined in Scheme 5, step IIb. We rationalize this process by formally decoupling the deprotonation and intersystem crossing into steps IIc and IId. Since the Ru center is in a +III oxidation state, the electron transferred to the quinone ligand originates from the newly formed oxo ligand. Comparing the Mulliken spin densities of $[(\mathbf{3/q}),(\mathbf{3/sq})]^{3+}_{T}$ and ${}^{b}[(\mathbf{3/sq}),(\mathbf{3/sq})]^{2+}_{T}$ we observe an increase of excess α-spin density from 0.34 to 0.98, while the spin density at the Ru2 center changes only slightly from 0.71 to 0.88. Thus, the electronic structure of ${}^{b}[(\mathbf{3/sq}),(\mathbf{3/sq})]^{2+}_{T}$ is best described as to contain two (sq)−Ru^{III}−$O^{\bullet}$ moieties. Intersystem crossing to the final open-shell singlet complex ${}^{b}[(\mathbf{3/sq}),(\mathbf{3/sq})]^{2+}_{OSS}$ gives no significant electronic structure change except the inversion of the spin orientations of the two halves of the complex to each other.

The relative ordering of the calculated pK_a values is somewhat surprising, as we may have expected the second deprotonation to be more demanding energetically, thus giving rise to a higher pK_a for the second acidic proton compared to the first. A closer inspection reveals, however, that the first proton originates formally from a Ru^{II}−OH_2 fragment, whereas the second is released from a Ru^{III}−OH moiety, invalidating the simplistic expectation based on the ease of deprotonation of water vs hydroxo groups. In addition, the energetically favorable intersystem crossing event mentioned above contributes to making the second proton more acidic and differentiating the first from the second proton abstraction.

Two-Electron Redox Behavior. Having identified the most plausible intermediates of the first two proton-coupled electron transfer process $[(\mathbf{2/sq}),(\mathbf{3/sq})]^{2+} \rightarrow {}^{b}[(\mathbf{3/sq}),(\mathbf{3/sq})]^{2+}_{OSS}$, we can calculate the associated redox potentials. Interestingly, the two oxidations are computed to be practically isoenergetic with the first being slightly more positive at a potential of 0.436 V than the second at 0.385 V vs Ag/AgCl. This energy ordering is interesting, as oxidations are expected to become increasingly more difficult and, thus, exhibit more positive redox potentials as the redox-active complex becomes more oxidized. If the second oxidation is associated with a less positive potential than the first, the multielectron redox process is said to exhibit potential inversion leading to a thermodynamically favorable disproportionation reaction summarized in eq 7.

$$2^{a}\left[\frac{3}{sq},\frac{3}{sq}\right]^{D}_{2+} \rightleftharpoons \left[\frac{2}{sq},\frac{3}{sq}\right]^{2+} + {}^{b}\left[\frac{3}{sq},\frac{3}{sq}\right]^{2+}_{OSS} \qquad (7)$$

This nonclassical behavior gives rise to a single two-electron current response in voltammetric experiments, and the observed $E_{1/2}$ is the average of the two individual potentials. Our calculations predict therefore a single two-electron wave response with a $E_{1/2}$ of 0.411 V vs Ag/AgCl in good agreement with the experimentally observed two-electron wave at ∼0.32 V in the cyclic voltammogram of Tanaka's complex. Why are the two oxidations so close in energy? Our analysis of the electron transfer process summarized in Scheme 5 provides an obvious explanation for the potential inversion. As pointed out above, the first electron is removed from the semiquinone moiety bound to Ru2 (step Ia). Subsequent deprotonation leads to an electronic reorganization where another electron from the $[Ru^{II/III}$−$(OH/OH_2)]$ conduit is pushed into the quinone moiety to formally recreate the Ru2−(semiquinone) fragment. This newly formed semiquinone moiety is again the redox-active component in the second oxidation (step IIa), and thus, both electrons originate from the π^* orbital of the semiquinone moiety illustrated in Figure 7. As a result, the electronic energies associated with the removal of the two electrons are practically identical at 116.9 and 118.1 kcal mol^{-1}, respectively. This intuitively understandable mechanism of controlling the redox potentials to establish a multielectron redox behavior is an interesting consequence of the redox noninnocent nature of the two Ru−(quinone) fragments that is unique to Tanaka's complex among the handful of examples of homogeneous water oxidation catalysts. The next two redox steps to complete the overall four-electron process are significantly more complicated and require a notably more detailed analysis. This work is currently in progress in our laboratory and will be reported elsewhere in due course.

■ CONCLUSIONS

For a better understanding of how Tanaka's complex promotes water oxidation under mild conditions, it is critically important that we delineate its redox properties and clearly identify which intermediates are involved in each of the redox steps. In particular, we have to identify at which point during the catalytic cycle the O−O bond may be formed and what mechanistic role the quinone ligands may play. Earlier studies

dx.doi.org/10.1021/ic102427g |Inorg. Chem. 2011, 50, 5946–5957

proposed that the O−O bond is formed at the first step when the starting complex is deprotonated.[27] In that scenario the metal centers are acting as a template and it is the quinone ligands which are oxidizing water to diruthenium bound μ-(O_2^{2-}). This is a real possibility, and our calculations confirm that it is energetically plausible if a strong base like ^{t}BuOK is present. In light of our plausible estimates of the first and second pK_a values, it is highly unlikely, however, that the deprotonation occurs at pH 4 in water. The UV−vis spectrum is deceptive since the doubly deprotonated species ($[(\mathbf{2/sq}),(\mathbf{2/sq})]^{0}_{T}$) and the AF coupled species ($[(\mathbf{2/sq}),(\mathbf{3/sq})]^{2+}$) may show similar transitions owing to the presence of a semiquinone unit in both cases. Our calculations suggest that only after the removal of two electrons can the two protons be removed from the terminal oxo groups at the plausible experimental pH to generate two terminal oxyl moieties in $^b[(\mathbf{3/sq}),(\mathbf{3/sq})]^{2+}$. At this stage the open-shell singlet is found to be lower in energy than the triplet. In the open-shell singlet state the unpaired electrons on the two terminal oxyl moieties have opposite spins and can readily couple to form the O−O bond.

On the basis of our detailed computational survey of all plausible intermediates, we propose that the O−O bond is *not* formed at the outset in water. The electronic ground state of the starting dihydroxo complex is better represented as the open-shell singlet ($[(\mathbf{2/sq}),(\mathbf{3/sq})]^{2+}$) where the unpaired spin densities on the metal and the ligand are antiferromagnetically coupled. This is a significant deviation from the current consensus, namely, that the ground state is a classical, closed-shell singlet species that we labeled and described as $[(\mathbf{2/q}),(\mathbf{2/q})]^{2+}$. Complex $[(\mathbf{2/sq}),(\mathbf{3/sq})]^{2+}$ ultimately gives rise to $^b[(\mathbf{3/sq}),(\mathbf{3/sq})]^{2+}_{OSS}$ via a two-electron, two-proton oxidation event computed to be at a potential of 0.411 V. In one of the two subunits the oxidation state of the ligand shuttles between 0 (quinone) and −I (semiquinone) while the oxidation state of the metal fluctuates between +II and +III, respectively, depending on the particular redox step.

■ ASSOCIATED CONTENT

Supporting Information. Additional discussions, more detailed schemes with additional intermediates considered, energy decomposition of the pK_a values discussed in the main text, comparisons of the energies of different spin states, Cartesian coordinates and vibrational frequencies of all species discussed. This material is available free of charge via the Internet at http://pubs.acs.org.

■ AUTHOR INFORMATION

Corresponding Author

*E-mail: mbaik@indiana.edu.

■ REFERENCES

(1) Lewis, N. S.; Nocera, D. G. *Proc. Natl. Acad. Sci.* **2006**, *103*, 15729–15735.
(2) Lewis, N. S.; Nocera, D. G. *Proc. Natl. Acad. Sci.* **2007**, *104*, 20142–20142.
(3) Barber, J. *Chem. Soc. Rev.* **2009**, *38*, 185–196.
(4) Pushkar, Y.; Yano, J.; Sauer, K.; Boussac, A.; Yachandra, V. K. *Proc. Natl. Acad. Sci.* **2008**, *105*, 1879–1884.
(5) Acho, J. A.; Doerrer, L. H.; Lippard, S. J. *Inorg. Chem.* **1995**, *34*, 2542–2556.
(6) Alstrum-Acevedo, J. H.; Brennaman, M. K.; Meyer, T. J. *Inorg. Chem.* **2005**, *44*, 6802–6827.
(7) Gust, D.; Moore, T. A.; Moore, A. L. *Acc. Chem. Res.* **2001**, *34*, 40–48.
(8) Gilbert, J. A.; Eggleston, D. S.; Murphy, W. R.; Geselowitz, D. A.; Gersten, S. W.; Hodgson, D. J.; Meyer, T. J. *J. Am. Chem. Soc.* **1985**, *107*, 3855–3864.
(9) Naruta, Y.; Sasayama, M.; Sasaki, T. *Angew. Chem., Int. Ed. Engl.* **1994**, *33*, 1839–1841.
(10) Ledney, M.; Dutta, P. K. *J. Am. Chem. Soc.* **1995**, *117*, 7687–7695.
(11) Limburg, J.; Vrettos, J. S.; Liable-Sands, L. M.; Rheingold, A. L.; Crabtree, R. H.; Brudvig, G. W. *Science* **1999**, *283*, 1524–1527.
(12) Sens, C.; Romero, I.; Rodriguez, M.; Llobet, A.; Parella, T.; Benet-Buchholz, J. *J. Am. Chem. Soc.* **2004**, *126*, 7798–7799.
(13) Zong, R.; Thummel, R. P. *J. Am. Chem. Soc.* **2005**, *127*, 12802–12803.
(14) Betley, T. A.; Wu, Q.; Voorhis, T. V.; Nocera, D. G. *Inorg. Chem.* **2008**, *47*, 1849–1861.
(15) Tseng, H.-W.; Zong, R.; Muckerman, J. T.; Thummel, R. *Inorg. Chem.* **2008**, *47*, 11763–11773.
(16) McDaniel, N. D.; Coughlin, F. J.; Tinker, L. L.; Bernhard, S. *J. Am. Chem. Soc.* **2008**, *130*, 210–217.
(17) Sartorel, A.; Carraro, M.; Gianfranco, S.; Zorzi, R. D.; Geremia, S.; McDaniel, N. D.; Bernhard, S.; Bonchio, M. *J. Am. Chem. Soc.* **2008**, *130*, 5006–5007.
(18) Concepcion, J. J.; Jurss, J. W.; Templeton, J. L.; Meyer, T. J. *J. Am. Chem. Soc.* **2008**, *130*, 16462–16463.
(19) Geletii, Y. V.; Botar, B.; Kögerler, P.; Hillesheim, D. A.; Musaev, D. G.; Hill, C. L. *Angew. Chem., Int. Ed.* **2008**, *47*, 3896–3899.
(20) Xu, Y.; Åkermark, T.; Gyollai, V.; Zou, D.; Eriksson, L.; Duan, L.; Zhang, R.; Åkermark, B.; Sun, L. *Inorg. Chem.* **2009**, *48*, 2717–2719.
(21) Even for the 'blue dimer', ligand based reactivity has been invoked. See the following to explain the isotope labeling experiment: Hurst; et al. *Inorg. Chem.* **2009**, *48*, 4400–4410.
(22) Ghosh, P. K.; Brunschwig, B. S.; Chou, M.; Creutz, C.; Sutin, N. *J. Am. Chem. Soc.* **1984**, *106*, 4772–4783.
(23) Wada, T.; Tsuge, K.; Tanaka, K. *Angew. Chem., Int. Ed.* **2000**, *39*, 1479–1482.
(24) Wada, T.; Tsuge, K.; Tanaka, K. *Inorg. Chem.* **2001**, *40*, 329–337.
(25) Remenyi, C.; Kaupp, M. *J. Am. Chem. Soc.* **2005**, *127*, 11399–11413.
(26) Kobayashi, K.; Ohtsu, H.; Wada, T.; Kato, T.; Tanaka, K. *J. Am. Chem. Soc.* **2003**, *125*, 6729–6739.
(27) Muckerman, J. T.; Polyansky, D. E.; Wada, T.; Tanaka, K.; Fujita, E. *Inorg. Chem.* **2008**, *47*, 1787–1802.
(28) Mukherjee, S.; Weyhermuller, T.; Bothe, E.; Wieghardt, K.; Chaudhuri, P. *Dalton Trans.* **2004**, 3842–3853.
(29) Kaim, W. *Dalton Trans.* **2003**, 761–768.
(30) Ringenberg, M. R.; Kokatam, S. L.; Heiden, Z. M.; Rauchfuss, T. B. *J. Am. Chem. Soc.* **2008**, *130*, 788–789.
(31) Vlugt, v. d.; Ivar, J.; Reek, J. N. H. *Angew. Chem., Int. Ed.* **2009**, *48*, 8832–8846.
(32) Ray, K.; Petrenko, T.; Wieghardt, K.; Neese, F. *Dalton Trans.* **2007**, 1552–1566.
(33) Hetterscheid, D. G. H.; Bas, d. B. *J. Mol. Catal.* **2006**, *251*, 291–296.
(34) Ward, M. D.; McCleverty, J. A. *Dalton Trans.* **2002**, 275–288.
(35) Pierpont, C. G.; Lange, C. W. *Progress In Inorganic Chemistry*; John Wiley & Sons: New York, 1993; Vol. 41, pp 331−442.
(36) Boyer, J. L.; Rochford, J.; Tsai, M.-K.; Muckerman, J. T.; Fujita, E. *Coord. Chem. Rev.* **2010**, *254*, 309–330.
(37) Rochford, J.; Tsai, M.-K.; Szalda, D. J.; Boyer, J. L.; Muckerman, J. T.; Fujita, E. *Inorg. Chem.* **2010**, *49*, 860–869.
(38) Yang, X.; Baik, M.-H. *J. Am. Chem. Soc.* **2006**, *128*, 7476–7485.
(39) Dede, Y.; Zhang, X.; Schlangen, M.; Schwarz, H.; Baik, M.-H. *J. Am. Chem. Soc.* **2009**, *131*, 12634–12642.
(40) Baik, M.-H.; Friesner, R. A. *J. Phys. Chem. A* **2002**, *106*, 7407–7415.
(41) *Jaguar 7.0*; Schrödinger, LLC: New York, 2007.

(42) Becke, A. D. *Phys. Rev. A* **1988**, *38*, 3098–3100.
(43) Becke, A. D. *J. Chem. Phys.* **1993**, *98*, 5648–5652.
(44) Vosko, S. H.; Wilk, L.; Nusair, M. *Can. J. Phys.* **1980**, *58*, 1200–1211.
(45) Lee, C. T.; Yang, W. T.; Parr, R. G. *Phys. Rev. B* **1988**, *37*, 785–789.
(46) Stephens, P. J.; Devlin, F. J.; Chabalowski, C. F.; Frisch, M. J. *J. Phys. Chem.* **1994**, *98*, 11623–11627.
(47) Hay, P. J.; Wadt, W. R. *J. Chem. Phys.* **1985**, *82*, 270–283.
(48) Wadt, W. R.; Hay, P. J. *J. Chem. Phys.* **1985**, *82*, 284–298.
(49) Dunning, T. H., Jr. *J. Chem. Phys.* **1989**, *90*, 1007–1023.
(50) Marten, B.; Kim, K.; Cortis, C.; Friesner, R. A.; Murphy, R. B.; Ringnalda, M. N.; Sitkoff, D.; Honig, B. *J. Phys. Chem.* **1996**, *100*, 11775–11788.
(51) Friedrichs, M.; Zhou, R. H.; Edinger, S. R.; Friesner, R. A. *J. Phys. Chem. B* **1999**, *103*, 3057–3061.
(52) Edinger, S. R.; Cortis, C.; Shenkin, P. S.; Friesner, R. A. *J. Phys. Chem. B* **1997**, *101*, 1190–1197.
(53) Rashin, A. A.; Honig, B. *J. Phys. Chem.* **1985**, *89*, 5588–5593.
(54) Noodleman, L. *J. Chem. Phys.* **1981**, *74*, 5737–5743.
(55) Noodleman, L.; Lovell, T.; Han, W.-G.; Li, J.; Himo, F. *Chem. Rev.* **2004**, *104*, 459–508.
(56) Noodleman, L.; Davidson, E. R. *Chem. Phys.* **1986**, *109*, 131–143.
(57) Tissandier, M. D.; Cowen, K. A.; Feng, W. Y.; Gundlach, E.; Cohen, M. H.; Earhart, A. D.; Coe, J. V.; Tuttle, T. R. *J. Phys. Chem. A* **1998**, *102*, 7787–7794.
(58) Tissandier, M. D.; Cowen, K. A.; Feng, W. Y.; Gundlach, E.; Cohen, M. H.; Earhart, A. D.; Tuttle, T. R.; Coe, J. V. *J. Phys. Chem. A* **1998**, *102*, 9308–9308.
(59) Zhan, C.-G.; Dixon, D. A. *J. Phys. Chem. A* **2001**, *105*, 11534–11540.
(60) Kelly, C. P.; Cramer, C. J.; Truhlar, D. G. *J. Phys. Chem. B* **2007**, *111*, 408–422.
(61) Fawcett, W. R. *Langmuir* **2008**, *24*, 9868–9875.
(62) Kelly, C. P.; Cramer, C. J.; Truhlar, D. G. *J. Phys. Chem. B* **2006**, *110*, 16066–16081.
(63) Supporting Information: Table ST1.
(64) Tsai, M.-K.; Rochford, J.; Polyansky, D. E.; Wada, T.; Tanaka, K.; Fujita, E.; Muckerman, J. T. *Inorg. Chem.* **2009**, *48*, 4372–4383.
(65) Rived, F.; Roses, M.; Bosch, E. *Anal. Chim. Acta* **1998**, *374*, 309–324.
(66) The electronic structure of the mono-deprotonated species is similar to the one reported previously by Muckerman et al. (ref 27).